EUROPEAN ORGANIZATION FOR NUCLEAR RESEARCH

CERN-EP/85-40
28 March 1985

DIMETHYL ETHER REVIEWED: NEW RESULTS ON USING THIS GAS IN A HIGH-PRECISION DRIFT CHAMBER

M. Basile, G. Bonvicini*), G. Cara Romeo, L. Cifarelli, A. Contin, G. D'Alì, C. Del Papa, G. Maccarrone, T. Massam, F. Motta, R. Nania, F. Palmonari, G. Rinaldi, G. Sartorelli, M. Spinetti, G. Susinno, F. Villa, L. Votano and A. Zichichi

Dipartimento di Fisica dell'Università, Bologna, Italy
Istituto Nazionale di Fisica Nucleare, Bologna, Italy
CERN, Geneva, Switzerland
Istituto Nazionale di Fisica Nucleare, LNF, Frascati, Italy
SLAC, Stanford, California, USA

ABSTRACT

Two years ago, dimethyl ether (DME) was presented, for the first time, as a suitable gas for high-precision drift chambers. In fact our tests show that resolutions can be obtained which are better by at least a factor of 2 compared to what one can get with conventional gases. Moreover, DME is very well quenched. The feared formation of whiskers on the wires has not occurred, at least after months of use with a 10 μCi ^{106}Ru source.

(Submitted to Nuclear Instruments and Methods in Physics Research)

---

*) Present address: Univ. of Michigan, Ann Arbor, Mich., USA.

1. INTRODUCTION

During the last few years the quest for higher and higher energies has placed more stringent demands on the performance of drift chambers, especially central/vertex detectors.

The momentum (p) resolution of a cylindrical drift chamber is given [1] by:

$$\frac{\delta p}{p} = \frac{\sqrt{750}}{\sqrt{(N+5)}} \frac{\delta s}{eBL^2} p \ .$$

In order to improve the momentum resolution, three quantities can be optimized in the design:

i) the transverse dimension of the chamber L
ii) the magnetic field B
iii) the spatial resolution of the chamber δs.

The transverse dimension L cannot be increased without paying a heavy price, since the number of wires (N) in the chamber and the size of the external devices (calorimeter etc.) will rapidly increase. The field B can only be increased up to 20 kG, before the iron-flux returns become saturated. In addition a large Lorentz angle will make it more difficult to design a working cell structure. If δs can be improved, we have none of the problems mentioned. A good spatial resolution is, on the other hand, the product of many factors: electron diffusion, statistics, geometry, systematics. One possible approach to improving δs is therefore to look for a gas with low electron diffusion at high reduced electric fields ($E/p \simeq 2$ V/cm.Torr). Since the diffusion coefficients and the drift velocity are correlated, in practice the gas with the smallest diffusion coefficient will have a small, non-saturated drift velocity.

This approach is, therefore, similar to that used by Walenta in his time expansion chamber [2].

A low drift velocity:

i) allows the use of the highest B fields without problems,
ii) affords the highest double-track resolution,
iii) requires a time resolution of 1 or 2 ns only.

On the negative side, a low drift velocity is impractical if the interaction rate is too high, while a non-saturated velocity will require either a constant drift field or a well-mapped-out space-time relation.

With the above facts in mind, we decided to explore the possibilities of dimethyl ether (DME), a gas already proposed two years ago for use in a high-resolution drift chamber [3].

2. DESIGN OF THE CHAMBER

Since the diffusion coefficient is a function of the drift field, it is desirable to operate at a value of the field such that the diffusion is at its minimum. On the other hand, the field on the wire necessary to have sufficient gain is a priori unknown. We needed, therefore, to design a system where the two fields could be changed independently. This has been achieved by making a drift space between an Al plate (at negative high voltage) and a transparent (grounded) wire mesh*). The eight sense wires (at positive high voltage) are 2.2 mm away from the mesh. In this way we have a long (30 mm) drift gap and a short (2.2 mm) gain gap (fig. 1). All the field non-uniformities are thus inside the gain gap. Aluminium plates at intermediate voltages, separated by insulated spacers, help shape the drift field [4] (fig. 2). Field wires are intended to reduce cross talk between sense wires. Sense and field wires are stretched on a printed-circuit (PC) board ending in a set of fingers to fit an electronic connector (fig. 3). A second PC board holds the wire mesh. Four threaded fibre-glass rods hold the Al plates and the PC boards together. The whole block is then screwed onto the lid of the outer vessel, by means of a teflon bracket in front and an Al box in the back. The necessary HV and signal connectors are also screwed onto the lid. The outer pressure vessel can be used up to 4 atm and it is entirely lined with teflon to prevent discharges. Finally all the HV resistors and capacitors are mounted on a fibre-glass board and epoxied to form a block with a connector to fit the PC board holding the wires.

3. BEAM SET-UP

We have used the t_{11} beam at the CERN Proton Synchrotron (PS). The beam momentum was set at 3.5 GeV/c. After focusing, the beam spot was only a few square centimetres, sufficient to give an approximately constant illumination of the chamber drift gap.

The beam divergence was small, approximately 20 mrad. A Cherenkov counter was used in anticoincidence to prevent electrons (i.e. electromagnetic showers) from producing triggers. Four scintillation counters were placed in the beam; two far upstream from the chamber and two right in front and behind it. A multi-wire proportional chamber (MWPC) was also placed in front of the chamber with wires orthogonal to the drift chamber wires. The beam slits have been kept almost entirely shut in order to reduce the chance of a two-track event.

---

*) Electroformed nickel mesh manufactured by Buckbee Mears, Minnesota, USA: thickness 25 μm; transparency 80%.

4. THE ELECTRONICS

The amplifiers (fig. 4) are contained in an Al box just outside the chamber. They have been designed with an emitter-follower as a front stage to close the wires on a resistance of ~ 400 Ω so as to get a large pulse and reduce the signal-to-thermal-noise ratio. The rest of the amplifier consists of two stages (Plessey SL560C) and a final emitter-follower to drive a 50 Ω cable. The amplification is about 10^2.

Once the signals reach the counting room, they are again amplified by a factor of 10 and discriminated (fig. 5). These delayed and shaped signals reach a multiplicity unit, which produces a LAM if there are at least n wires hit within the maximum drift time and if the veto has been lifted by the occurrence of a coincidence among four scintillation counters (see below). In addition one MWPC wire is required in the trigger in order to select tracks along a short part (4 mm), in the middle of the sense wires.

When a track crosses the chamber, the time-to-digital converter (TDC) (an LRS 4208 with extended range, least significant bit = 1 ns, needing no calibration) is enabled, a START signal reaches the COMMON input, and the wire signals can (with a minimum delay of ~ 150 ns) reach the individual STOPs. An END OF WINDOW signal is eventually generated by a second timing unit, after which no new hit is accepted by the system until the event is read out and cleared.

5. THE GAS SYSTEM

Since we used pure DME, we kept the bottle with its pressure reducer close to the chamber. Input pressure was simply read on the manometer of the pressure reducer. On the chamber output there was a second pressure reducer followed by a flowmeter, and a bubbler located outside the beam area to monitor the gas flow.

For the runs with a mixture of Ar and CO_2 we used a standard EP gas rack.

6. DATA TAKING

Data were taken in a variety of conditions. We started with an admixture of Ar and CO_2 as a bench-mark. The parameters subject to variations were: the drift field E, the gas pressure p, and the number of wires hit (n) required in the trigger. During data taking, we were able to monitor the distributions of drift times and of the quantity $x = (t_1 + t_3)/2 - t_2$ for any three adjacent wires by means of on-line histograms. As is obvious, the average x is zero and the width of its distribution is related to the time resolution.

7. METHOD OF ANALYSIS

To calculate the spatial resolution, we need to reconstruct tracks (using eight points) and calculate residuals. To do that, we transform times into distances from the mesh (y), by means of the drift velocity (W). The drift velocity is known from the drift time and the drift-gap length (see fig. 6), where the drift time is the difference between the maximum drift time and the drift time in the gain gap. This last time is reasonably easy to determine given the peculiar shape of the time distribution of tracks going through the gain gap. This shape is due to the fact that there are two gain gaps (one to the left and one to the right of the sense wires) and to the fact that the high, non-saturated drift velocity in the gain gaps squeezes the events into few bins. The determination of the boundary of the gain-gap is also important for the rejection of tracks crossing it, which are not analysed in this paper because of their complicated space-time relation. Time-walk corrections were not applied. We suspect these corrections to be non-negligible.

The efficiency of the chamber has also been calculated from the data. Since we request n (typically 5) wires in the trigger, we are guaranteed that there is a track going through the chamber. The efficiency is therefore given by the ratio N/N_{tot}, where N is the number of tracks seen by the wire and N_{tot} is the number of tracks seen by the chamber.

8. RESULTS

Figures 7a and b show the results for the drift velocity. Both in the case of Ar/CO_2 and in the case of DME, the results are consistent with previously measured values within a few per cent [2, 5, 6]. Major causes of errors may have been a non-perfect control of the pressure and temperature of the gases. The values of the velocities are shown in table 1.

Figure 8 shows a typical spatial-residual distribution. Figures 9a, b, and c, show the behaviour of the spatial resolution plotted against $\sqrt{\langle \text{distance} \rangle}$ from the mesh at given electric field and pressure. We have fitted the data with straight lines: $\sigma = a \sqrt{\langle y \rangle} + b$, and collected the values of a and b, for the different operating conditions, in table 1.

This choice of fit is explained below. Let us define s, δs, and ds, respectively, as the path length, the r.m.s. fluctuation of the path length, and an infinitesimal path length. Let σ_L be the diffusion coefficient: $\delta s = \sigma_L \sqrt{y}$. The total time resolution (δt) is given by two contributions: one in the drift field $\delta s/W$, due to diffusion; and one in the gain gap, due to diffusion,

geometry, and statistics, $\delta[\int ds/W_g(s)]$ (the integral is extended from the mesh to the wire surface); i.e. $\delta t^2 = (\delta s/W)^2 + \{\delta[\int ds/W_g(s)]\}^2$. Therefore the space resolution is $\sigma^2 = (\delta s)^2 + W^2 \{\delta[\int ds/W_g(s)]\}^2$. Evidently the contribution of the gain gap is depressed by a factor W/W_g and hopefully negligible. If that were the case: $\sigma \approx \sigma_L \sqrt{y}$. The proportionality coefficient between σ and σ_L depends on statistics and electronics and, in general, has not been well controlled during the runs, because of the change of discriminators, thresholds, etc. Examining the data, one finds that a constant b must be added, i.e. the contribution of the gain gap is not always negligible, although at 2.7 atm, $b \approx 0$ indeed. It is interesting to note that b is proportional to W in the Ar/CO_2 data, while in the DME data the correlation is more complicated.

The values a of the slopes are plotted (fig. 10) against the drift field. These slopes follow the behaviour of σ_L with the drift field, as shown by a comparison with published data [2, 5].

Finally, fig. 11 shows the resolution obtained with an admixture of Ar and CO_2 (76:24) in the same chamber. The resolution here is at least a factor of 2 worse than what we have in DME at 1 atm. However, in the worst case (high drift field, short drift path) the gain is more like a factor of 5. Presumably in a real central/vertex detector the drift field will have to be rather high to keep the Lorentz angle at a manageable value; thus a factor of 3 to 5 is more representative of a realistic situation.

9. CONCLUSIONS

We have found DME to be a well-behaved, well-quenched, and stable gas. The voltage-holding properties of the chamber have not changed with time, indicating that there was no growth of whiskers. The measured velocities are consistent with those measured by other groups. It must be pointed out that the spatial resolution is dominated by the diffusion coefficient, as proved both by the linear behaviour of the resolution as a function of $\sqrt{\langle \text{distance} \rangle}$ and by the behaviour of the slope of the fits as a function of drift field. Evidently, this shows that the search for a low-diffusion gas was justified. Notice that the slopes of the fits to the Ar/CO_2 data are higher than the DME ones by a factor of 2. From published values of diffusion coefficients, we would have expected this factor to be higher ($\sim$ 5). In addition the value of the slope a of the 2.7 atm data is much bigger than can be explained taking into account the worsening of the diffusion at low electric field, which should, anyway, be partially offset by the increase in pressure.

In conclusion, it seems fair to say that although the pattern of our data is qualitatively comprehensible, probably a second level of analysis (to take

into account, for instance, deformations at the level of 0.1% of the tracks due to the non-constant drift field) as well as a Monte Carlo study will be necessary. Also, as already pointed out, we have not even attempted to analyse the tracks going through the gain gap. The spatial resolutions seem to be a factor of 2 to 5 better than what is obtained with a classical mixture. The efficiency with DME was always very close to 100%.

Acknowledgements

We would like to express our appreciation to the technical services of the INFN (Bologna), for designing the chamber (G. Laurenti and C. Alvisi) and for designing and testing the amplifiers (P. Montanari and R. Volta). Our thanks go also to the technicians who built the pressure vessel, and to H. Bienkowski for building the drift cell and helping to solve many other problems. The help of the Muratori group, and especially of J.C. Bertrand, L. Bassi and R. Harfield, is also gratefully acknowledged. J. Va'vra has been so kind as to lend us his program to map the electric field.

REFERENCES

[1] R.L. Gluckstern, Nucl. Instrum. Methods 24 (1963) 381.

[2] J. Fehlman et al., The time expansion chamber, *in* Proc. Int. Conf. on Instrumentation for Colliding Beam Physics, Stanford, 1982 (SLAC-250, Stanford, 1982), p. 34.

[3] F. Villa, Nucl. Instrum. Methods 217 (1983) 273.

[4] J. Va'vra, Nucl. Instrum. Methods 217 (1983) 322.

[5] A. Peisert and F. Sauli, Drift and diffusion in gases: a compilation, CERN 84-08 (1984).

[6] J. Fehlmann and G. Viertel, Compilation of data for drift chamber operation (ETH, Zurich, 1983).

Table 1

Values of the parameters a and b as a function of $\sqrt{\langle y \rangle}$ for both DME and Ar/CO_2. Also shown are drift velocities.

E/p (V/cm.Torr)	W (μm/ns)	a (μm/√cm)	b (μm)	Gas
1.3	2.71 ± 0.05	27 ± 1	2 ± 1	DME
1.75	3.86 ± 0.13	14 ± 1	13 ± 5	DME
1.9	4.68 ± 0.02	18 ± 2	21 ± 2	DME
2.37	5.88 ± 0.05	19 ± 4	22 ± 5	DME
3.15	7.75 ± 0.07	20 ± 7	28 ± 8	DME
0.7	15 ± 1	43 ± 12	44 ± 11	Ar/CO_2
1.4	37 ± 2	36 ± 12	72 ± 8	Ar/CO_2
2.1	58 ± 2	36 ± 15	97 ± 13	Ar/CO_2

Figure captions

Fig. 1a,b,c : Cross-section of the chamber. 1: Pressure vessel. 2: Lid. 3: Board holding the mesh. 4: Board holding the wires. The thickness of these boards (2.2 mm) forms the gain gaps. 5: Fibre-glass spacers. A nylon-threaded rod goes through these spacers and Al plates (7), is screwed in the Al (grounded) box in the back (9), and is tightened by a nut (not shown) on the front Al plate (6). 6: Front Al plate, closing the drift space. 7: Field-shaping Al plates, with a rectangular cut-out to permit the electron drift towards the wires. 8: Teflon pedestal to fasten the drift cell to the vessel lid. 9: Al box supporting the drift-cell structure in the back. 10: Epoxy box, containing decoupling HV resistors and condensers. The wire-supporting board is inserted in an appropriate connector to bring the HV to the field and sense wires.

Fig. 1d : The outside of the chamber is shown. It is easy to recognize the final pressure reducer and the flowmeter. The plexiglas box in front of the pressure vessel contains the resistor chain. Cables (not shown) bring the HV to the connectors visible on the lid.

Fig. 1e : The Al plates forming the drift cell are clearly visible. The white cables bring the HV to the plates or to the wire (via the epoxy box visible in the back). The black Lemo cables bring the signals out. Other details visible are the large conical teflon pieces covering the HV connectors, the fibre-glass spacers, the Al box in the back, and the teflon support in front.

Fig. 2a : Drift lines. The track is parallel to the plane of wires. Plates are simulated with thick wires. Clearly visible are the sense/field wires and the grid.

Fig. 2b : Equipotentials in the proximity of the wires. Notice the uniformity of the field.

Fig. 3 : High-voltage decoupling scheme. All resistors and condensers are epoxied into a block. The external connections are done

with two PC connectors (to wires and amplifiers) or banana connectors (HV in). Wire diameters are respectively 20 μm and 100 μm for sense and field wires.

Fig. 4 : Simplified scheme of the front-end electronics.

Fig. 5 : Trigger and acquisition electronics.

Fig. 6 : Time distribution. Dividing the drift-gap width (30 mm) by the drift time (t = 7.83 μs in this case), we get the drift velocity (3.83 μm/ns in this case). Operating conditions: E/p = 1.75 V/cm.Torr, p = 2 atm. The final values of velocities come from the average on all wires and all data sets, taken under the same operating conditions.

Fig. 7a : Drift velocity in Ar/CO_2 (76:24) at 1 atm. The curves at 80:20 and 70:30 come from Ref. 6.

Fig. 7b : Drift velocity in pure DME plotted against reduced electric field.

Fig. 8 : Typical residual distribution. Same operating conditions as in fig. 6. FWHM = 53 μm, σ = FWHM/2.35 = 22 μm.

Fig. 9a,b,c : Spatial resolution as a function of $\sqrt{\langle \text{distance} \rangle}$ from mesh in DME, respectively at 1 atm, 2 atm, 2.7 atm. We combine all the wires together, and assuming the same relationship we calculate average and errors. We have divided the distance into four bins: 1-7.5 mm, 7.5-15 mm, 15-22.5 mm, and 22.5-30 mm.

Fig. 10 : Behaviour of the slope of the fits in figs. 9a, b. This is in fact a measurement of the diffusion coefficient. Dashed line and triangle points come respectively from ref. 5 (p. 125) and ref. 2. In both cases, the data have been normalized to our point at E/p = 2.37 V/cm.Torr. In addition, the slope of the data at E/p = 1.75 V/cm.Torr (p = 2 atm) has been multiplied by a factor of $\sqrt{2}$ to take into account the increase of a factor of 2 in pressure.

Fig. 11 : Spatial resolution as a function of $\sqrt{\langle \text{distance} \rangle}$ from mesh in Ar/CO_2 at 1 atm, for three values of the drift field. Fitted curves are again straight lines. Notice that the slopes of the fits are very nearly the same, indicating constancy of the diffusion coefficients as a function of drift field. Such 'saturation' of the diffusion coefficient is consistent with known data.

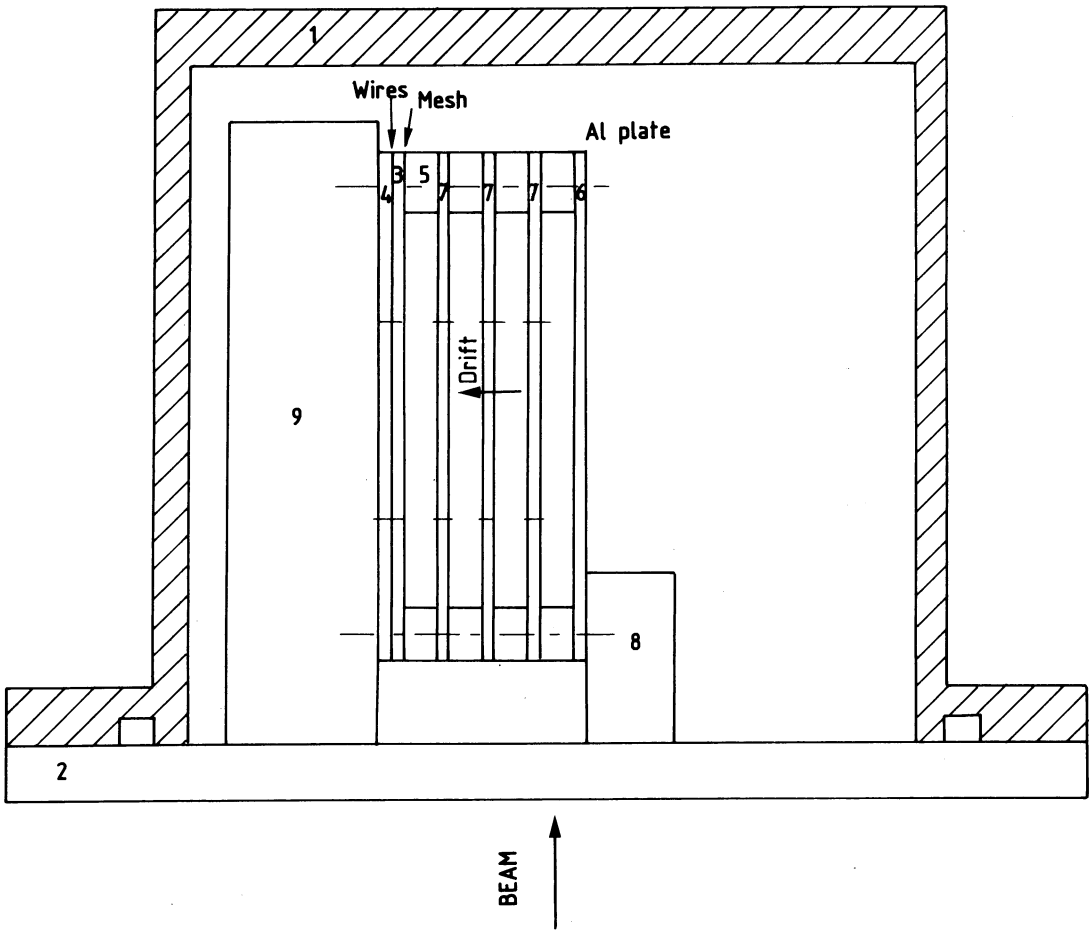

Fig. 1a

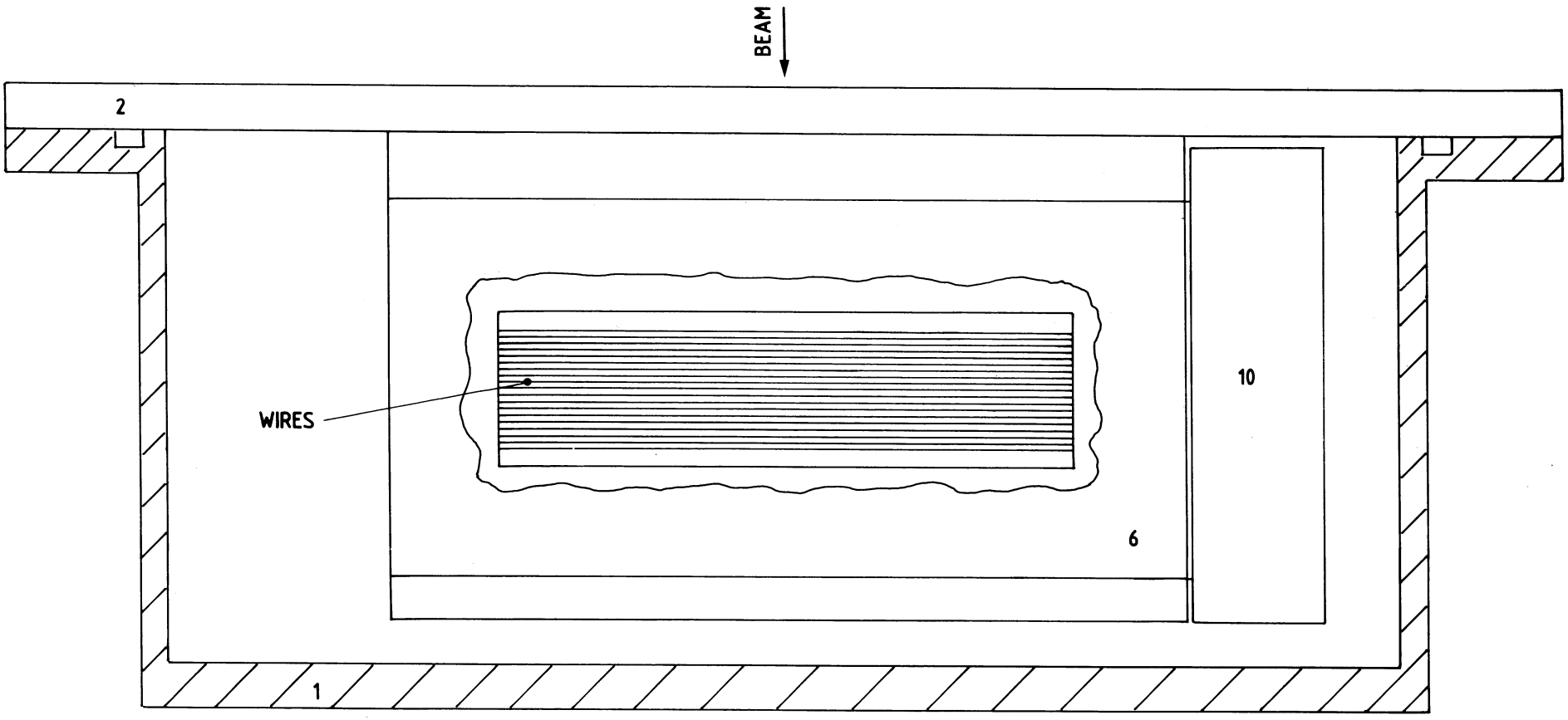

Fig. 1b

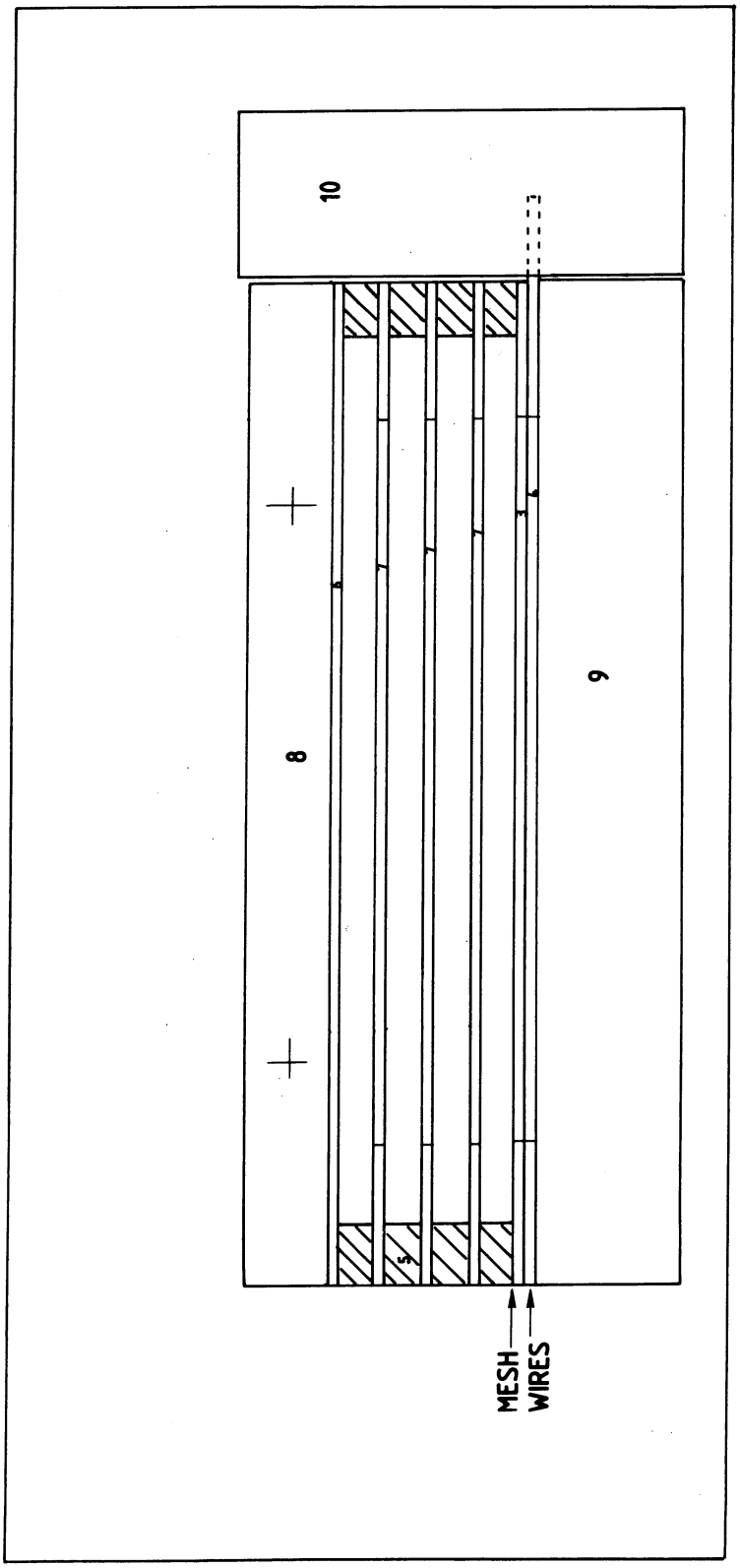

Fig. 1c

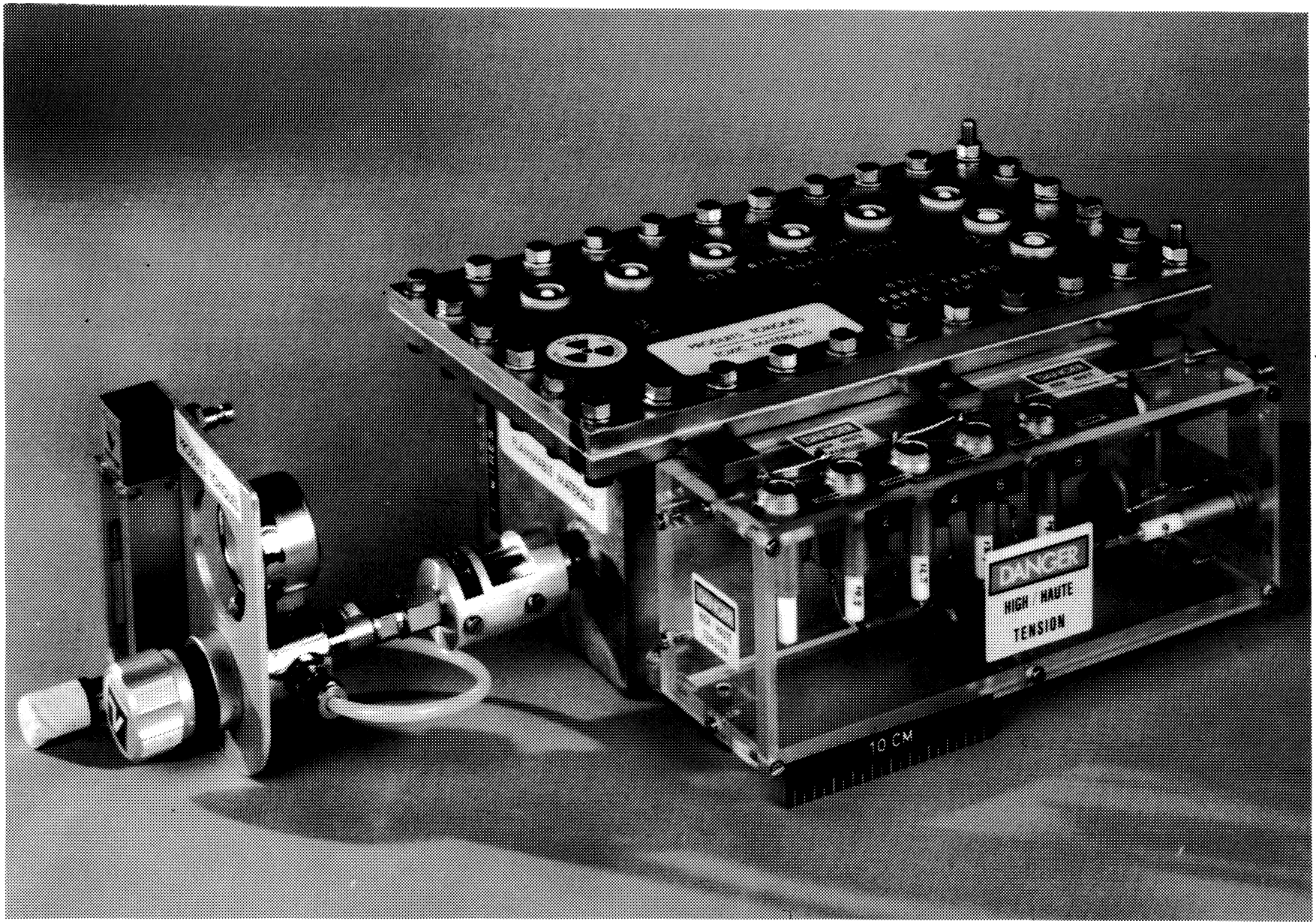

Fig. 1d

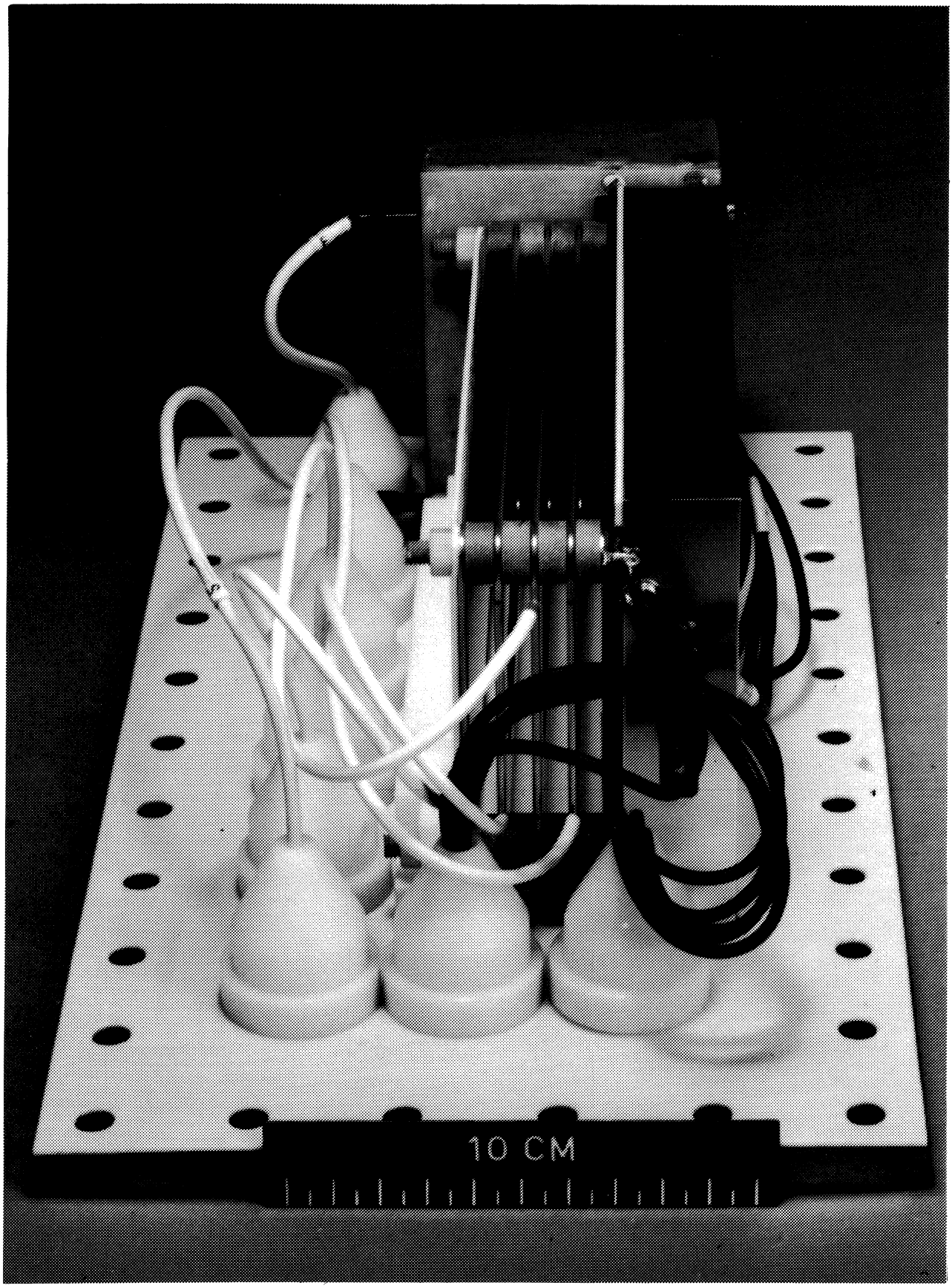

Fig. 1e

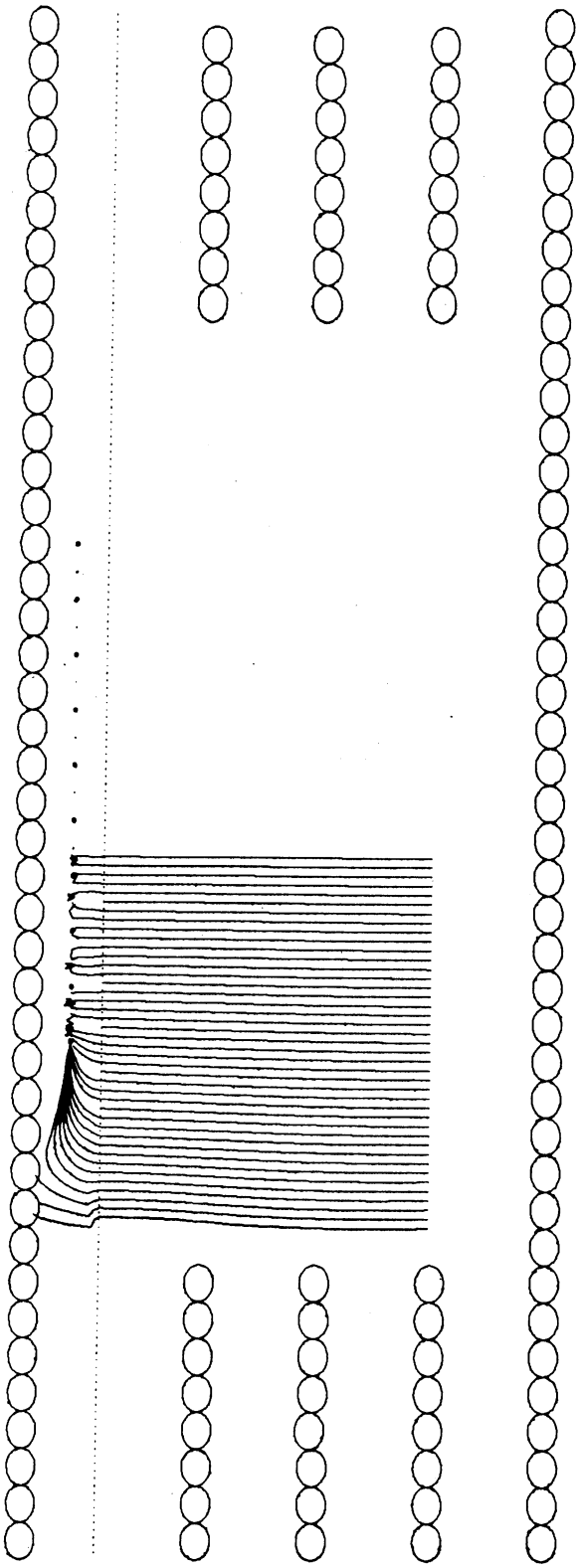

Fig. 2a

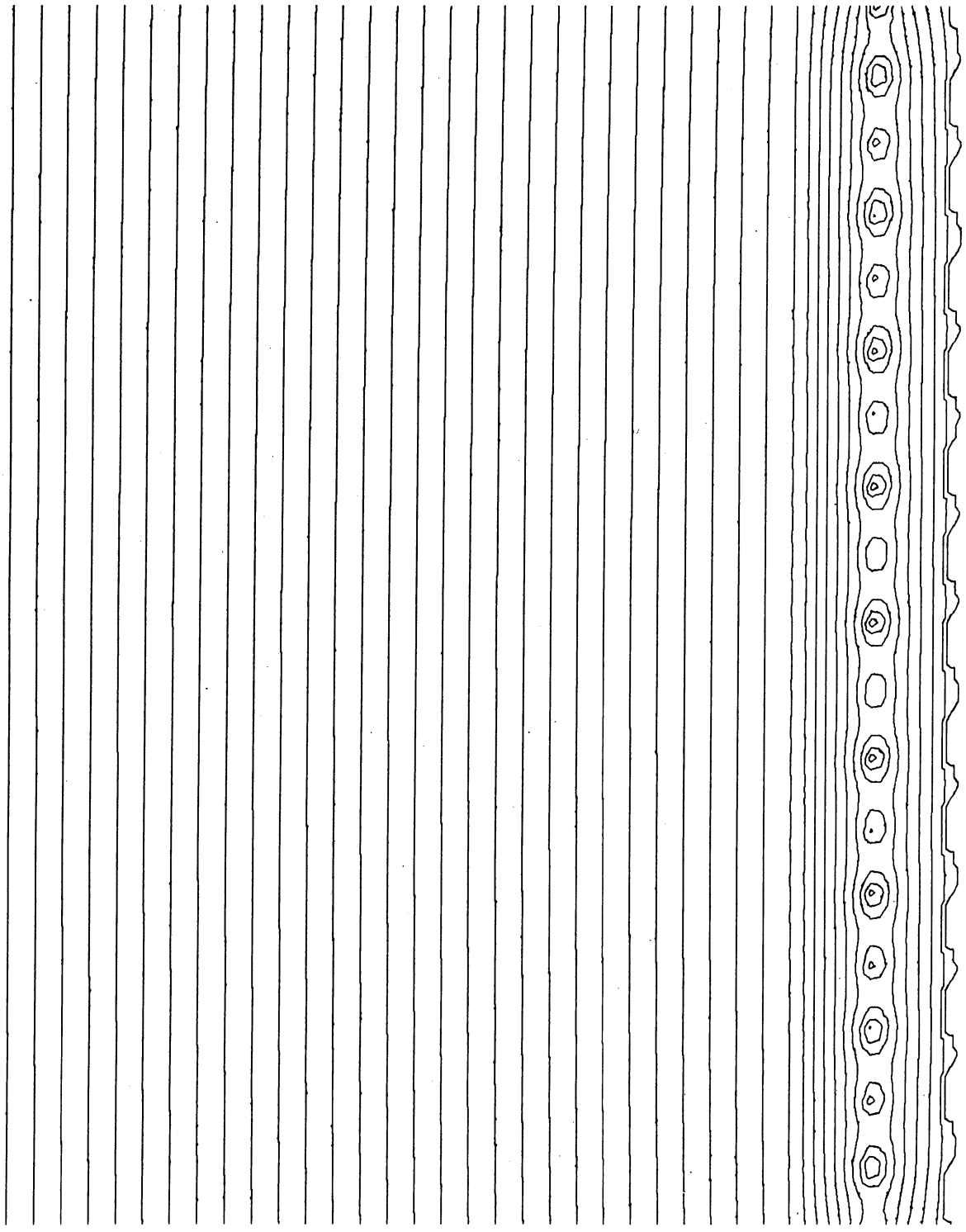

Fig. 2b

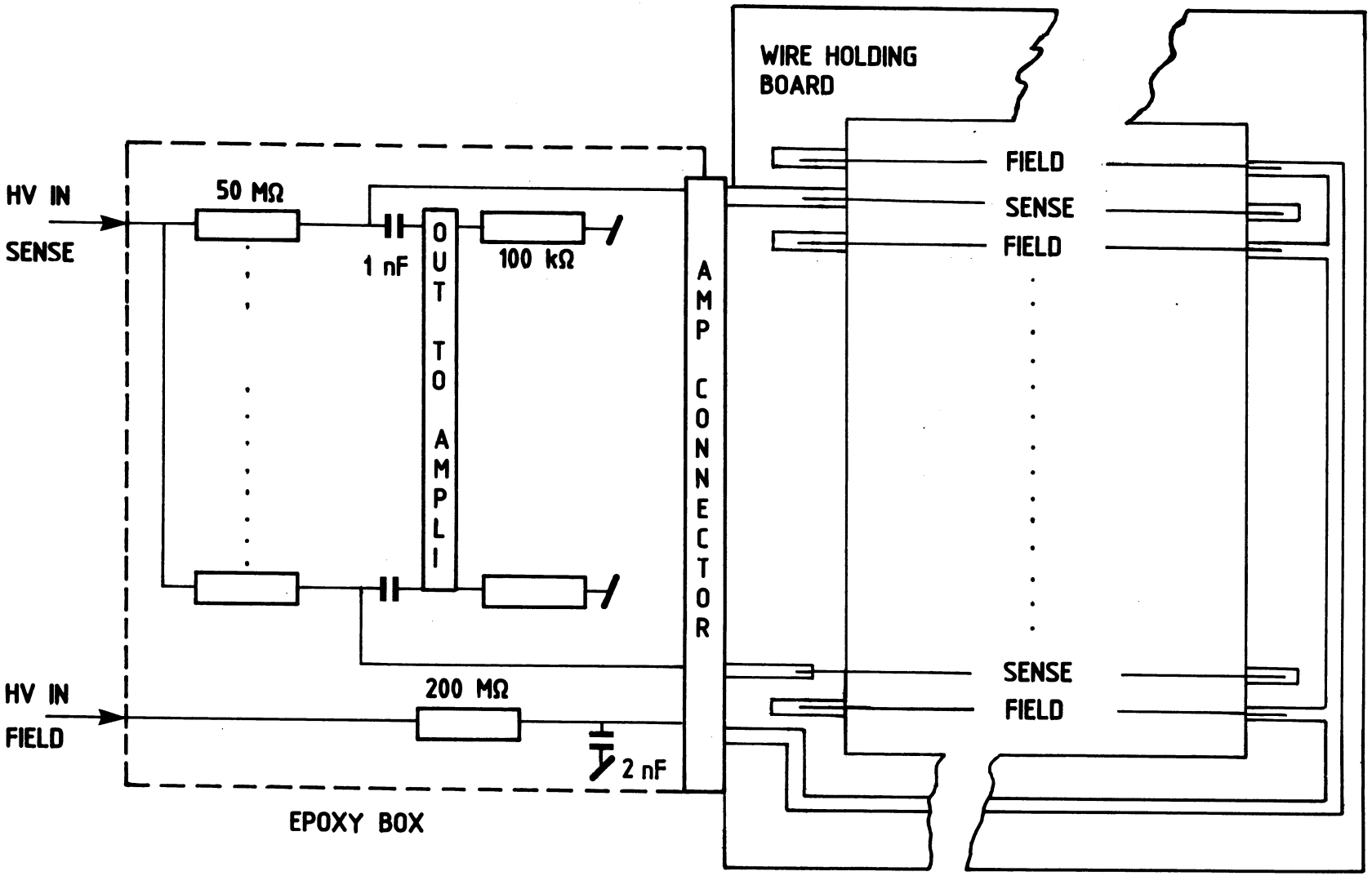
WIRE HOLDING
BOARD
HV IN
SENSE
50 MΩ
1 nF
OUT TO AMPLI
100 kΩ
AMP CONNECTOR
FIELD
SENSE
FIELD
SENSE
FIELD
HV IN
FIELD
200 MΩ
2 nF
EPOXY BOX

Fig. 3

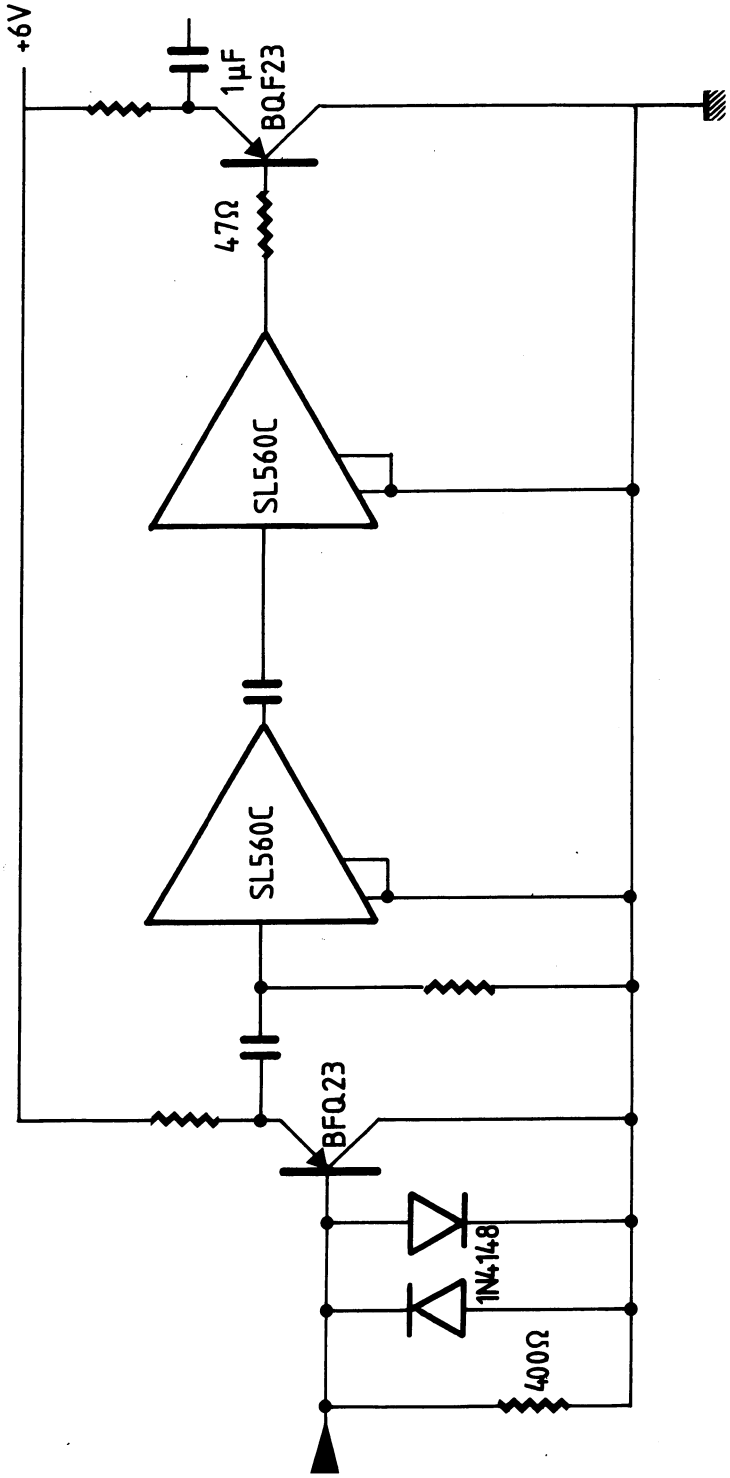

Fig. 4

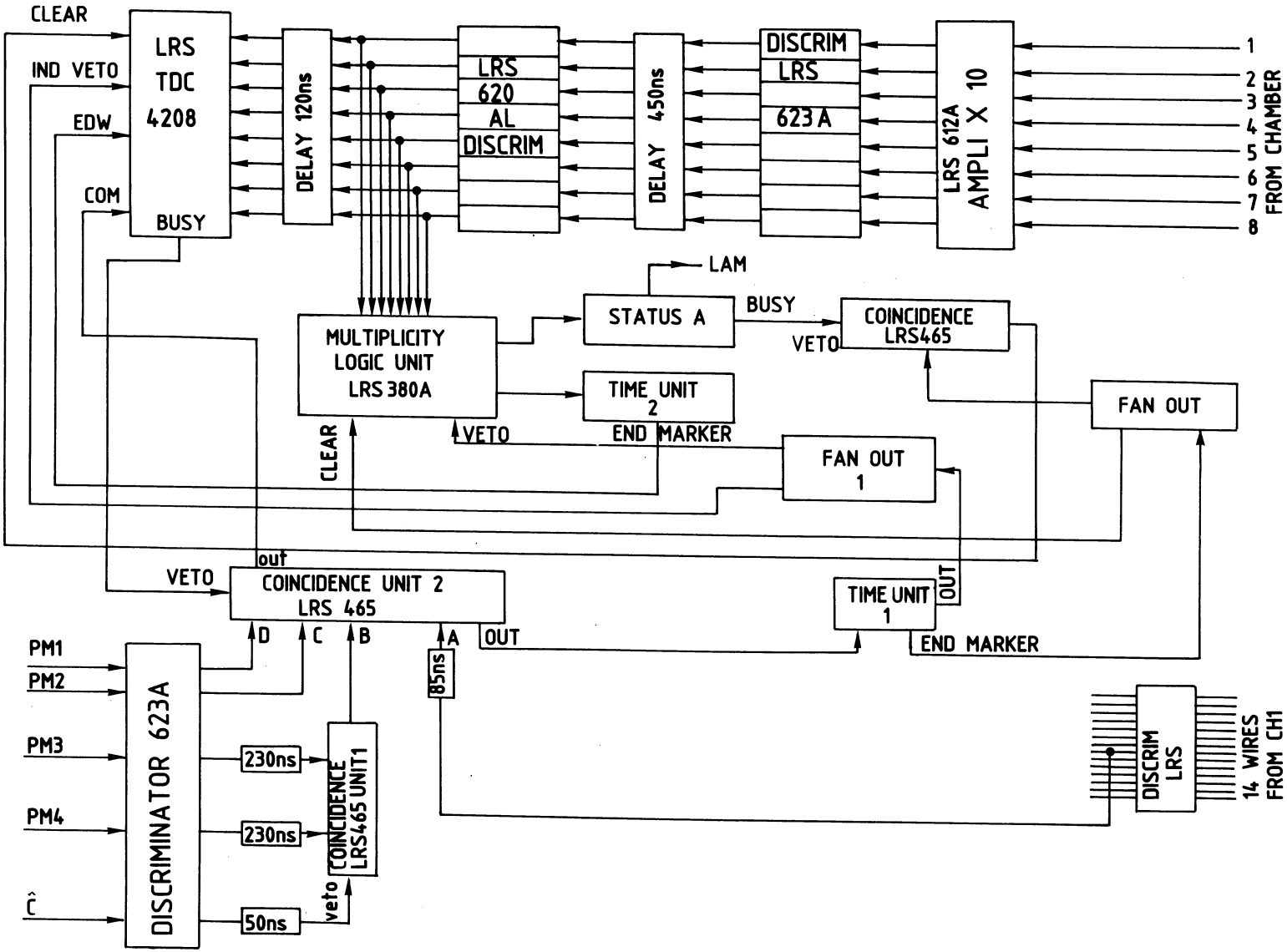
CLEAR
IND VETO
EDW
COM
LRS TDC 4208
BUSY
DELAY 120ns
LRS 620 AL DISCRIM
DELAY 450ns
DISCRIM LRS 623A
LRS 612A AMPLI X 10
1
2
3
4
5
6
7
8
FROM CHAMBER
LAM
STATUS A
BUSY
COINCIDENCE LRS465
VETO
MULTIPLICITY LOGIC UNIT LRS 380A
TIME UNIT 2
VETO
END MARKER
FAN OUT
FAN OUT 1
CLEAR
out
VETO
COINCIDENCE UNIT 2 LRS 465
D
C
B
A
OUT
TIME UNIT 1
OUT
END MARKER
PM1
PM2
PM3
PM4
DISCRIMINATOR 623A
230ns
230ns
50ns
COINCIDENCE LRS465 UNIT1
veto
85ns
DISCRIM LRS
14 WIRES FROM CH1

Fig. 5

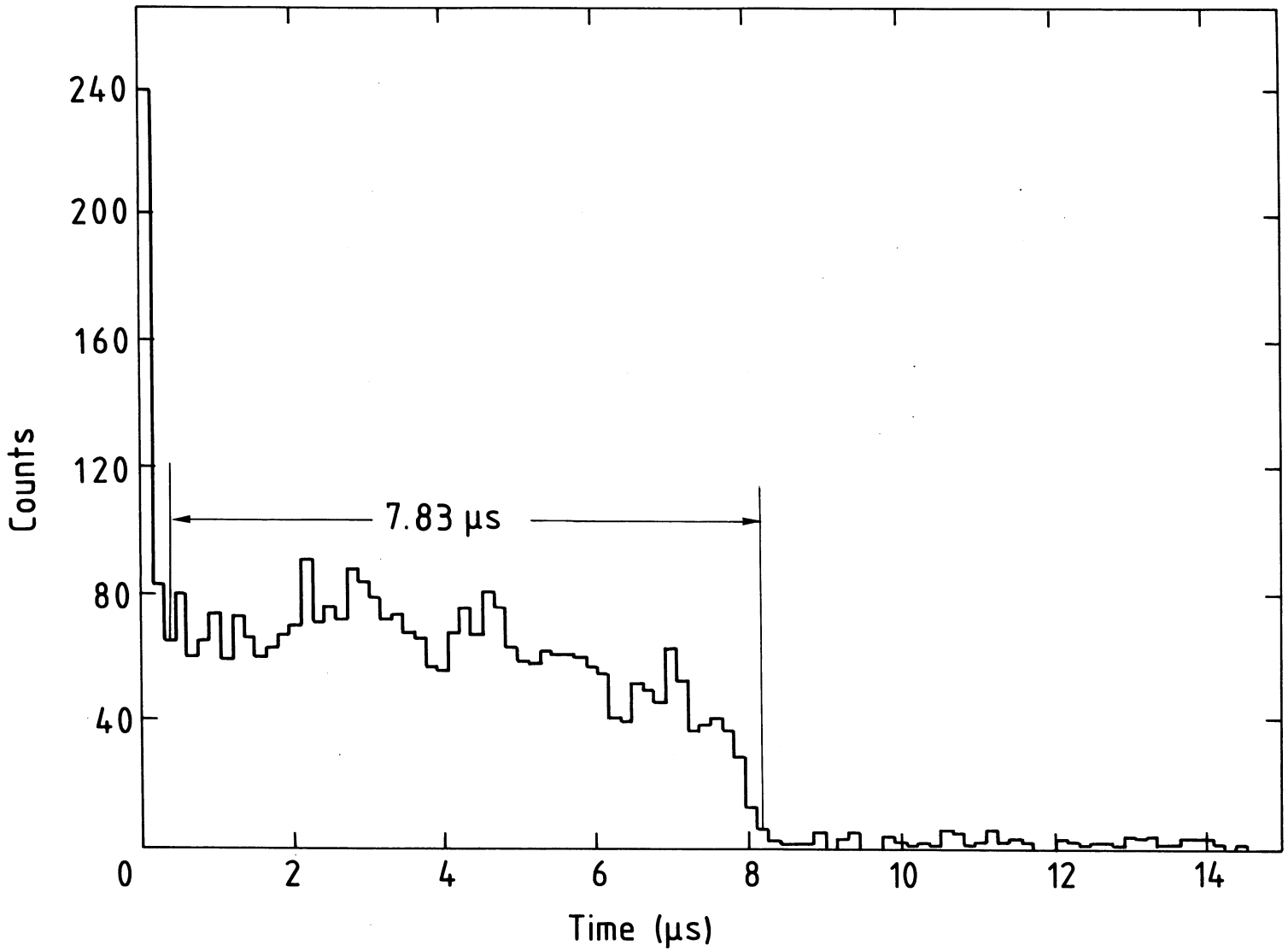

Fig. 6

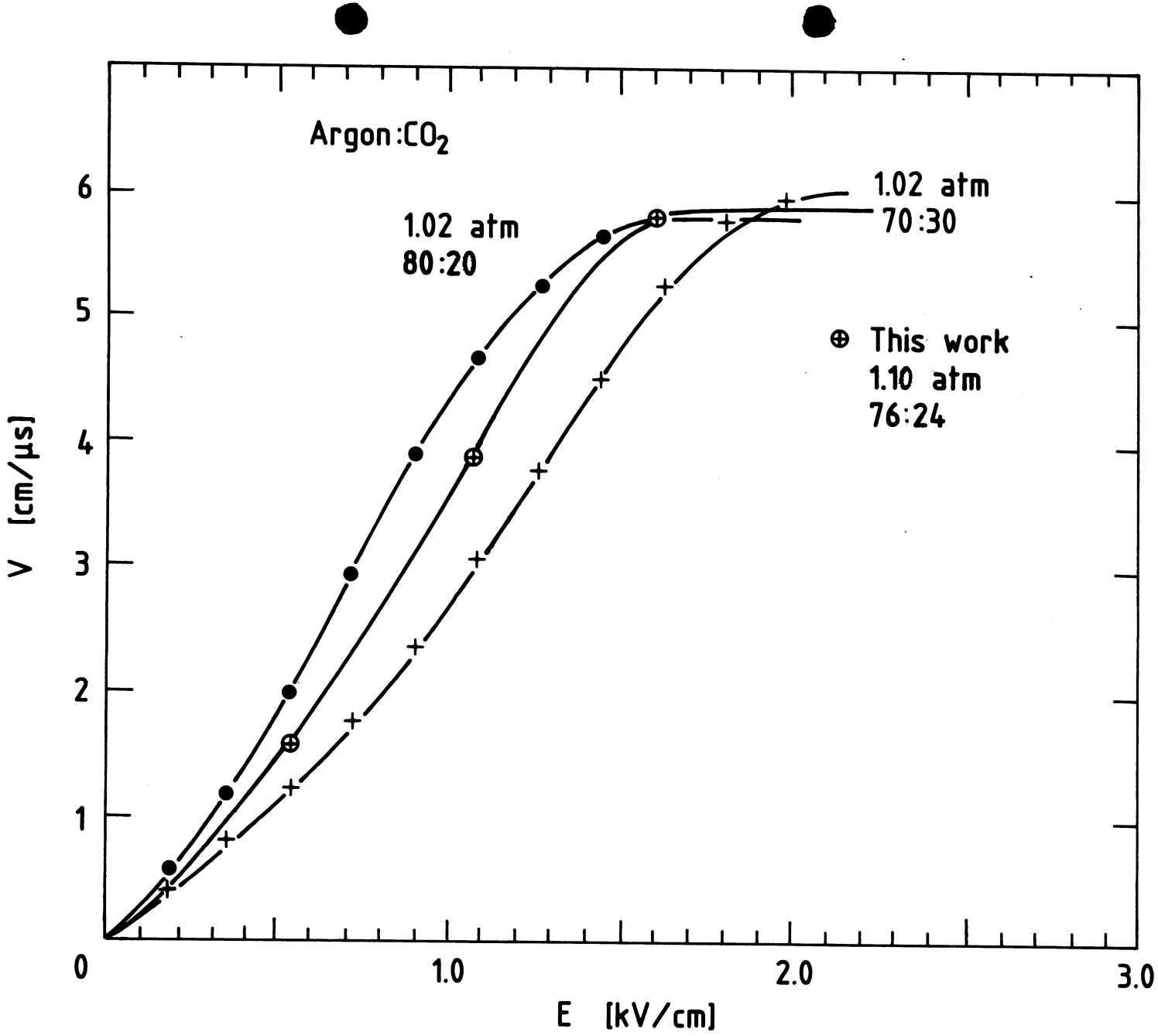
Argon:CO_2
1.02 atm
80:20
1.02 atm
70:30
⊕ This work
1.10 atm
76:24
V [cm/μs]
E [kV/cm]
0
1.0
2.0
3.0
1
2
3
4
5
6

Fig. 7a

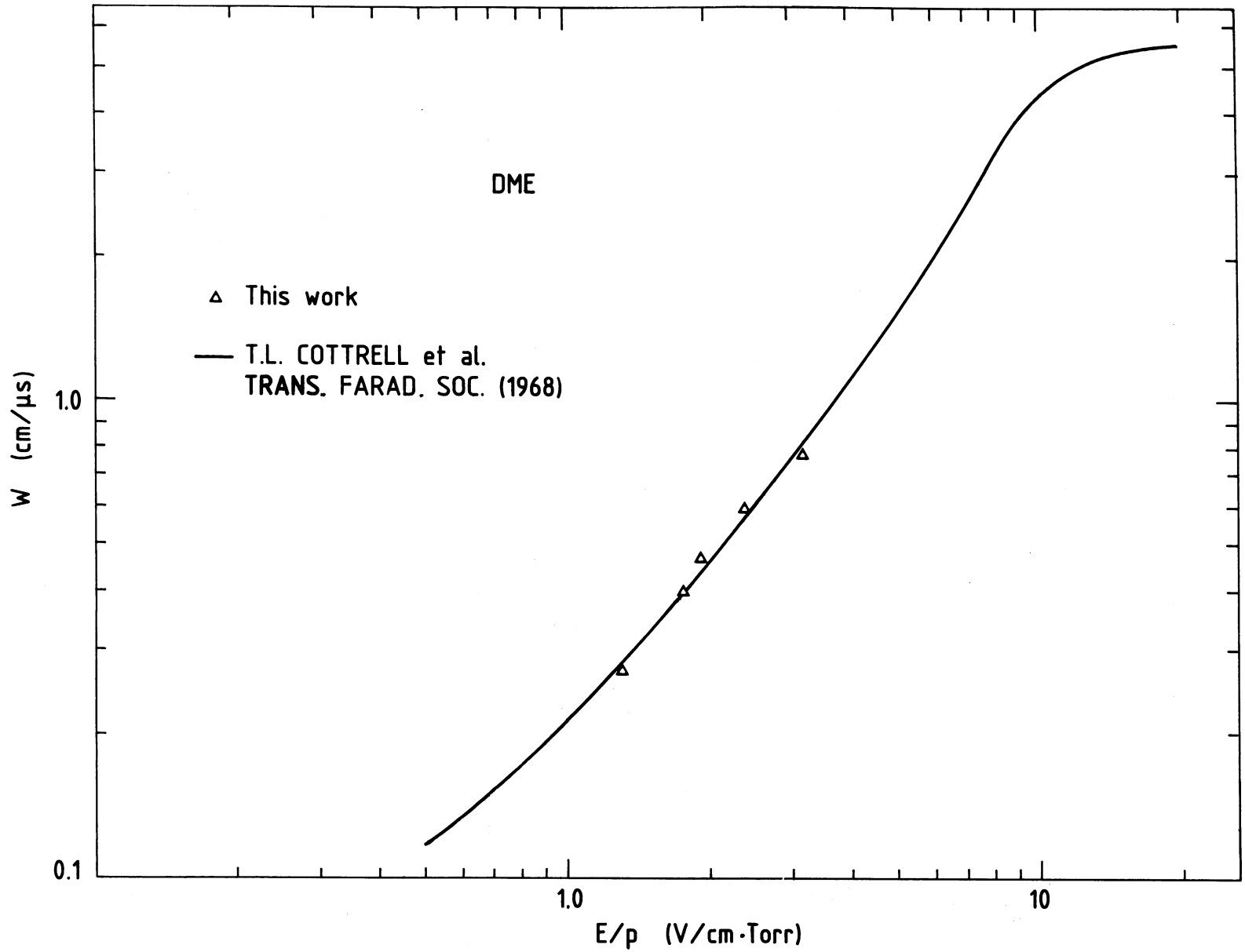
DME
This work
T.L. COTTRELL et al.
TRANS. FARAD. SOC. (1968)
W (cm/μs)
1.0
0.1
1.0
10
E/p (V/cm·Torr)

Fig. 7b

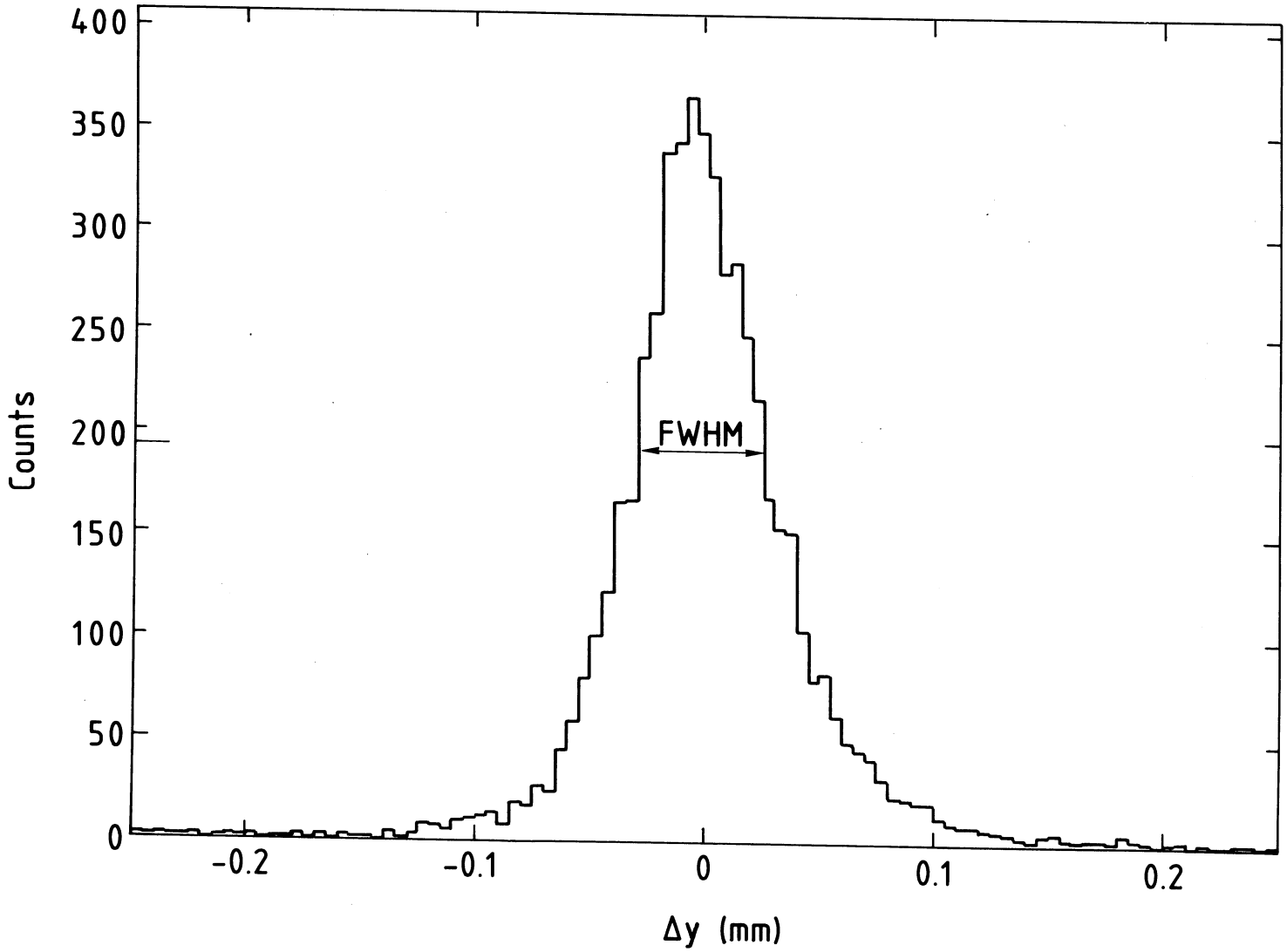

Fig. 8

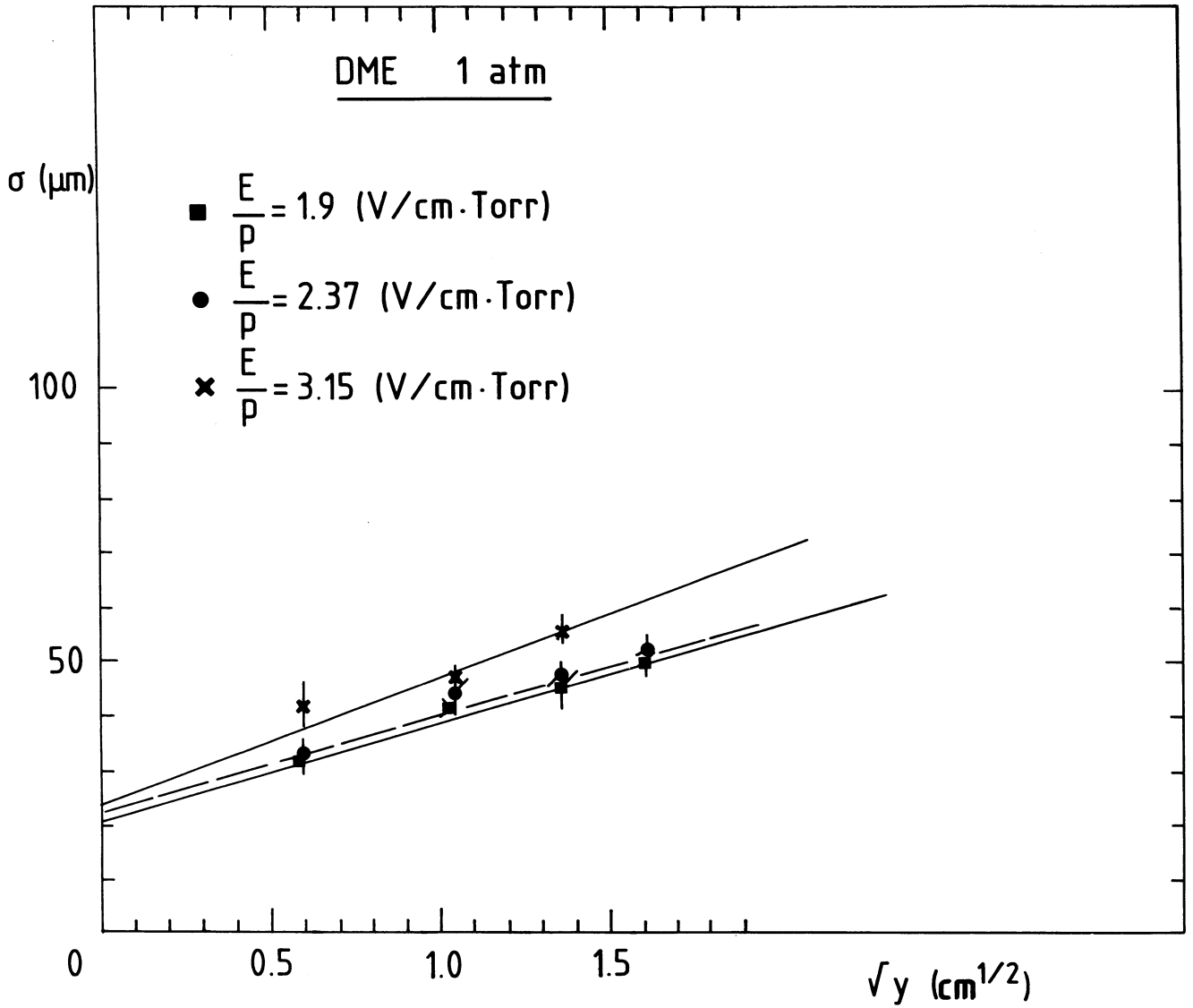
DME 1 atm
σ (μm)
■ E/p = 1.9 (V/cm·Torr)
● E/p = 2.37 (V/cm·Torr)
✖ E/p = 3.15 (V/cm·Torr)
100
50
0
0.5
1.0
1.5
√y (cm^1/2)

Fig. 9a

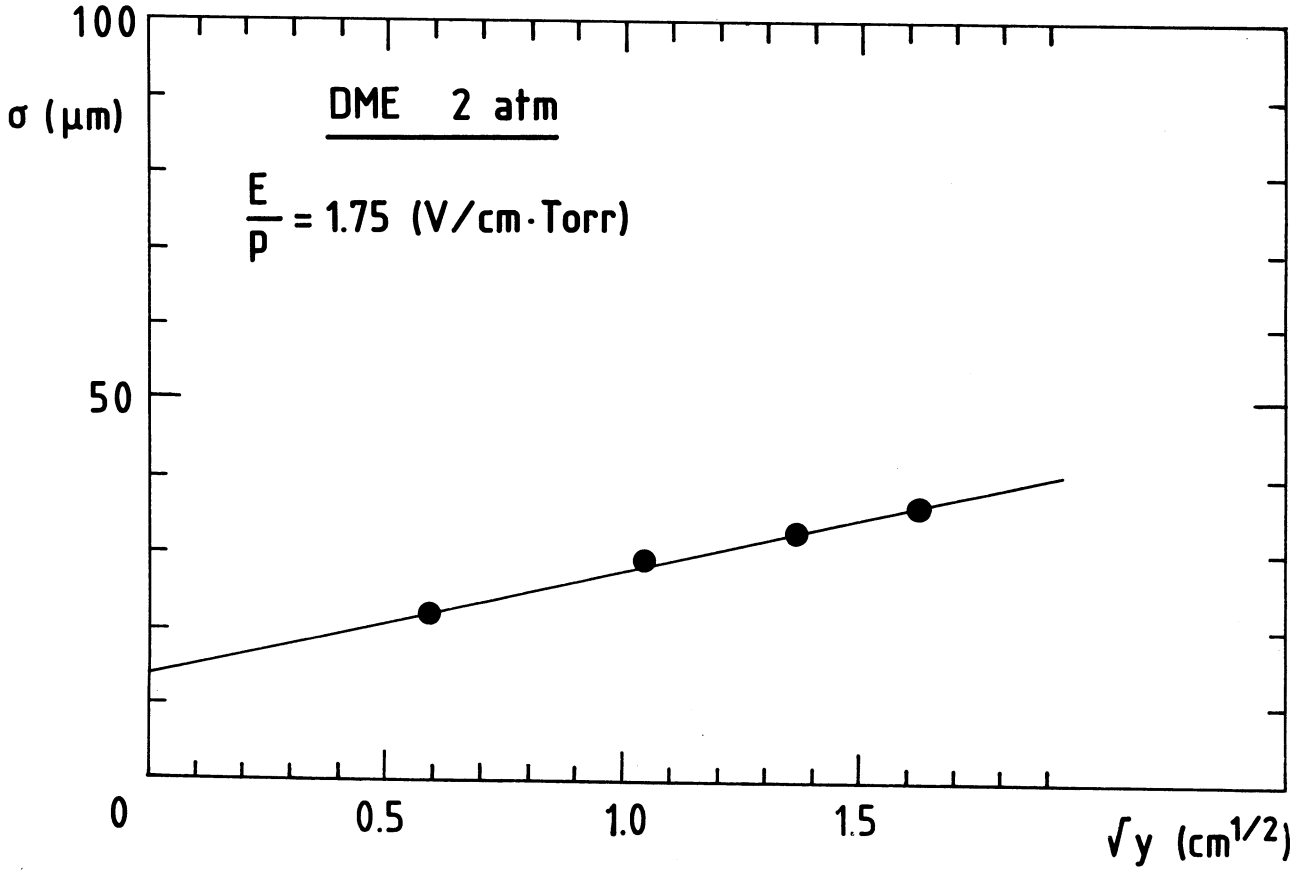

Fig. 9b

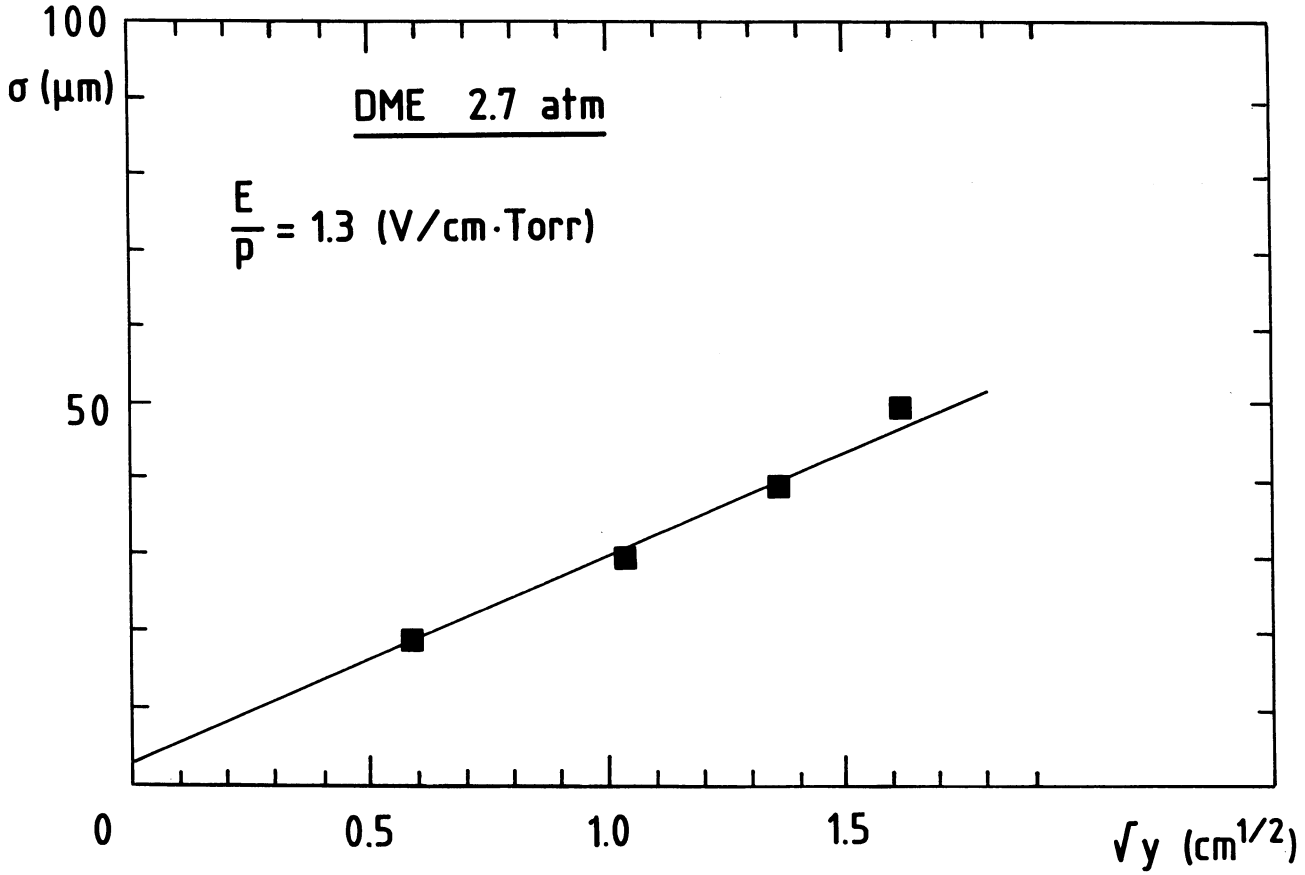

Fig. 9c

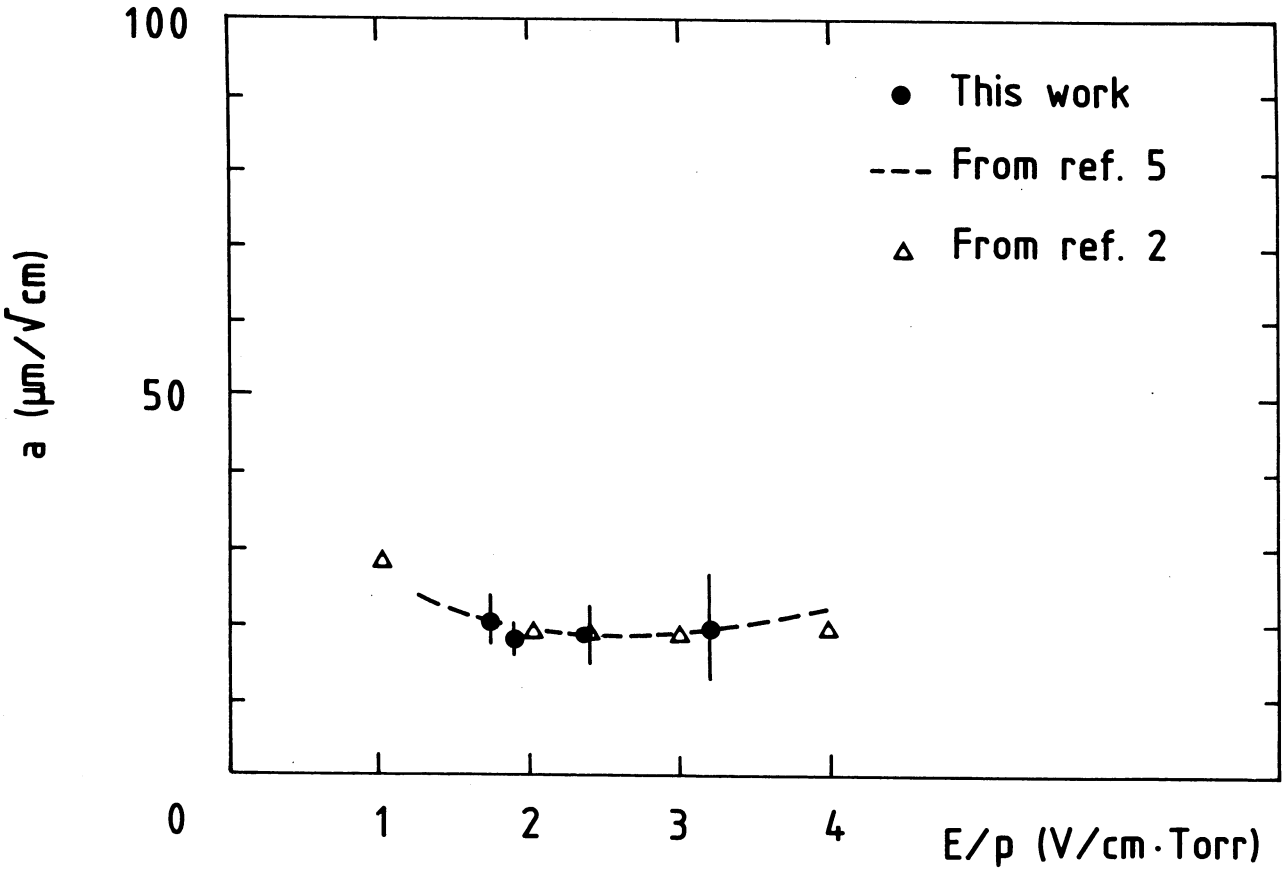

Fig. 10

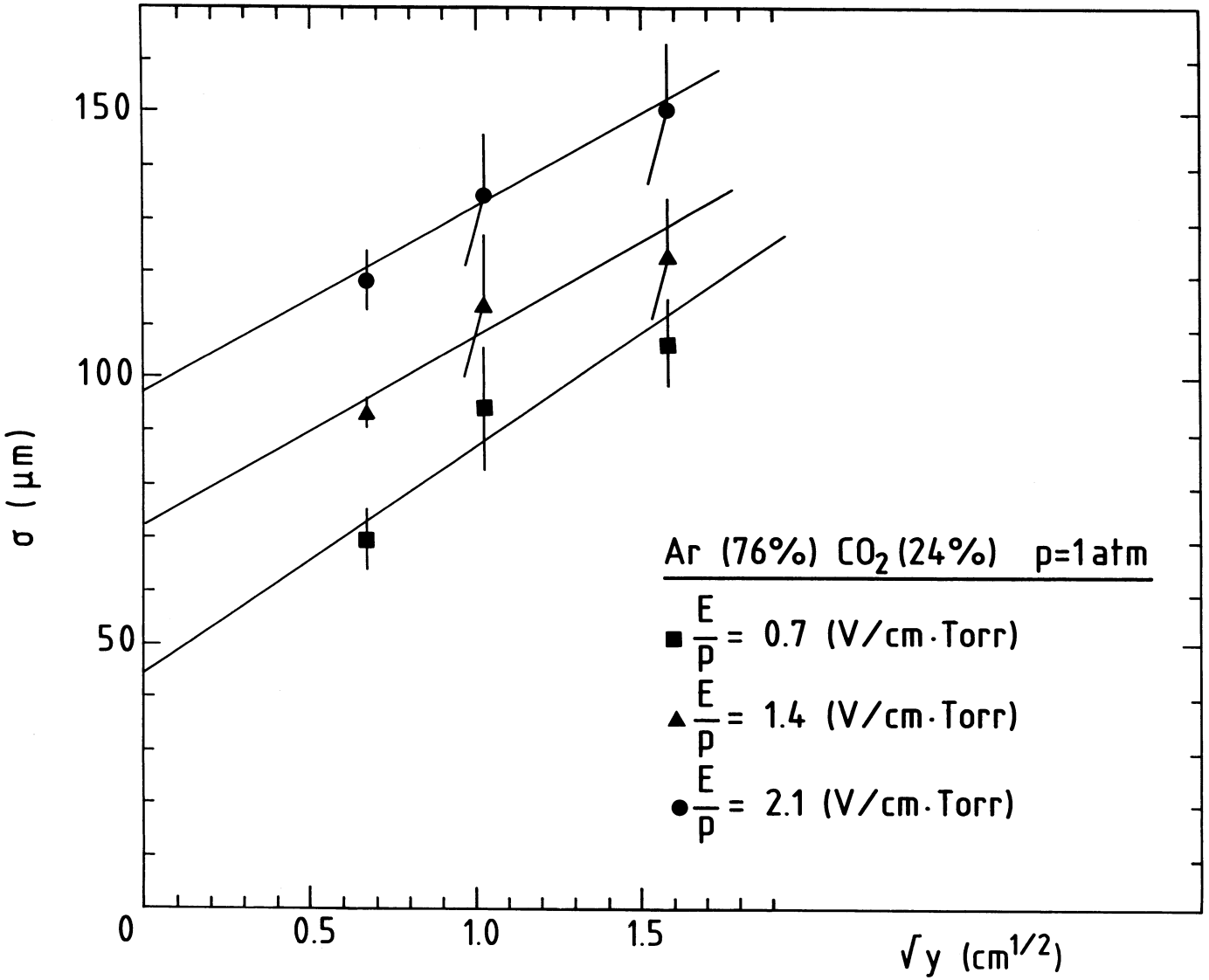
150
100
50
0
0.5
1.0
1.5
σ (μm)
√y (cm^1/2)
Ar (76%) CO2 (24%) p=1atm
■ E/p = 0.7 (V/cm·Torr)
▲ E/p = 1.4 (V/cm·Torr)
● E/p = 2.1 (V/cm·Torr)

Fig. 11